



Article

Manifestation of the Early 20th Century Warming in the East-European Plain: Atmospheric Circulation Anomalies and Its Connection to the North Atlantic SST and Sea Ice Variability

Valeria Popova ^{1,*}, Tatiana Aldonina ^{1,2} and Daria Bokuchava ^{1,2}

¹ Institute of Geography, Russian Academy of Sciences, Moscow 119017, Russia

² A.M. Obukhov Institute of Atmospheric Physics, Russian Academy of Sciences, Moscow 119017, Russia

* Correspondence: valeria_popova@mail.ru; Tel.: +7-(915)-3410414

Abstract: A study of the climatic characteristics and annual runoff of the Volga and Severnaya Dvina rivers demonstrates that, on the East European Plain (EEP), Early Twentieth Century Warming (ETCW) manifested in a multiyear drought between 1934 and 1940; this drought has no analogues in this region in terms of intensity and duration according to Palmer’s classification, and caused extreme hydrological events. The circulation conditions during this event were characterized by an extensive anticyclone over Eastern Europe, combined with a cyclonic anomaly in the circumpolar region. An analysis of the spatial features of sea surface temperature (SST) anomalies indicate that the surface air temperature (SAT) anomalies in July on the EEP during ETCW were related not only to the North Atlantic (NA) warming and positive AMO phase, but also to a certain spatial pattern of SST anomalies characteristic of the 1920–1950 period. The difference between the SST anomalies of the opposite sign in the different NA zones, used as the indicator of the obtained spatial pattern, shows the quite close relations between the July SAT anomalies on the EEP and the atmospheric circulation patterns responsible for them. The positive phase of the Atlantic Multidecadal Oscillation (AMO) and the expansion of the subtropical high-pressure belt to the north and to the east can be considered as global-scale drivers of this phenomenon. The AMO also impacts the sea ice cover in the Barents–Kara Sea region, which, in turn, could have led to specific atmospheric circulation patterns and contributed to droughts on the EEP in the 1930s.

Keywords: early 20th century warming; East-European Plain; Volga and Severnaya Dvina basins; river runoff; extremes; drought; drivers; atmospheric circulation; AMO; SST anomalies



Citation: Popova, V.; Aldonina, T.; Bokuchava, D. Manifestation of the Early 20th Century Warming in the East-European Plain: Atmospheric Circulation Anomalies and Its Connection to the North Atlantic SST and Sea Ice Variability. *Atmosphere* **2023**, *14*, 428. <https://doi.org/10.3390/atmos14030428>

Academic Editor: Michael L. Kaplan

Received: 15 November 2022

Revised: 10 February 2023

Accepted: 17 February 2023

Published: 21 February 2023



Copyright: © 2023 by the authors. Licensee MDPI, Basel, Switzerland. This article is an open access article distributed under the terms and conditions of the Creative Commons Attribution (CC BY) license (<https://creativecommons.org/licenses/by/4.0/>).

1. Introduction

ETCW is the second positive climatic anomaly comparable in magnitude to modern warming, whose mechanisms still remain a matter of scientific debate. An analysis of the regional climate anomalies recorded during this period reveals the opportunity to study the mechanisms of internal natural climate variability and the causes of the occurrence of such anomalies in association with the global changes that characterize ETCW.

A sharp rise in the temperature of the ocean surface, particularly in the NA and the AMO anomalies, with the peak of its positive phase in the 1930s, is recognized as the main factor of the ETSW [1–3]. To date, catastrophic droughts, accompanied by the “Dust Bowl” phenomena in the 1930s in the U.S. Great Plains, have been thoroughly studied [3–7]. The three-dimensional analysis of regional and large-scale atmospheric circulation patterns demonstrates that ocean impact was the major driving force behind these phenomena; this primarily includes the SST anomalies of the NA, which contributed to the formation of abnormal spatial circulation patterns in the mid-troposphere and a flow over North America toward the Atlantic in the upper-troposphere [4]. Other research has highlighted an anomalous continental-wide circulation pattern that resulted in the occurrence of a blocking anticyclone that forced extreme warming over the Great Plains [6]. In turn, heat

wave activity, caused by an anomalously warm NA, was enhanced through the feedbacks associated with dry spring conditions, de-vegetation and soil moisture deficiency [5–7]. Study [8] suggests that dust storms in North America were primarily forced by the SST variability, not excluding the factor of human-induce land degradation.

Regional anomalies, such as the Dust Bowl droughts in the 1930s, have been associated with low-frequency changes in the planetary atmospheric circulation, in particular, the shift in the northern Hadley cell and the northern tropical belt towards the pole [3,9]. The southward shift in the northern tropical belt since the mid-1940s has been widely recognized as a driver of droughts in central Europe in the 1940s–1950s [10]. The consequences of the catastrophic flooding of the Mississippi in 1927, which made thousands of people homeless and significantly affected the social life of the American North, have also been investigated [11].

Studies on the regional manifestations of ETCW in the mid- and high-latitudes of Eurasia have been mainly focused on the winter season and the problem of reducing the Arctic Sea ice, as well as the related atmospheric circulation anomalies [3,12,13]. At the same time, the unprecedented rise and decrease in the annual runoff of the Volga and the Northern Dvina rivers recorded in the long-term series of hydrological observations indicate that there were large-scale anomalies of humidification in 1920–1940. A brief analysis of these phenomena was presented in [14]. In this paper, we study the causes of the changes in the hydro-climatic characteristics during these events, focusing on the relationship between the atmospheric circulation patterns seen with the NA warming and the Arctic sea ice variations, considering them in the context of ETCW.

2. Materials and Methods

The study of humidification anomalies on the EEP in 1920–1940 is based on long-time series observational data on the changes in the annual runoff of the Severnaya Dvina river (at Ust-Pinega), as well as the Volga (Volgograd) and its tributaries, the Vyatka (Kirov), Belya (Birsk), and Oka (Kaluga) rivers (Figure 1). Spatial averaged (20–60 E; 45–70 N) data from observational gridded archives are also examined: the monthly temperature, using HadCRUT5.0 [15] and GISTEMP v4 [16], precipitation, using CRU TS4.05 [17] and the Palmer Drought Severity Index (PDSI), using CRU-scPDSI [18].

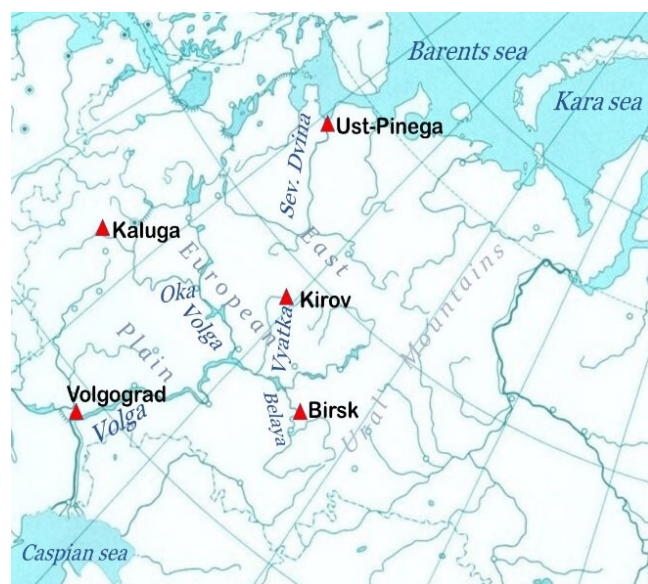


Figure 1. Location of the hydrological stations (red triangles).

An analysis of the empirical orthogonal functions (EOFs) of the variability in the atmosphere sea-level pressure anomalies was used to reveal the circulation patterns that are responsible for the formation of heat and drought conditions on the EEP, according to

observations from the HadSLP2 grid archive [19]. An analysis of the AMO time series and SST anomalies, based on the HadSST.4.0.0.0 data set [20], was focused on the contribution of the NA to the sharp change in the temperature and humidification regime on the EEP in 1920–1940.

We also analyzed the possible link between sea ice variability in the Barents–Kara Sea region, and the warm and drought conditions on the EEP in 1920–1940, using correlation analysis (both synchronous and shift); this used the monthly mean sea ice area in the Barents Sea, the sea ice extent (SIE) in the Kara Sea, the SST and the sea-level pressure (SLP).

SIE data in August for the Kara Sea, covering the period since 1924, was obtained from the Arctic and Antarctic Research Institute database [21]. Since no such long-series in situ data are available for the Barents Sea, we used a new modified version of the reconstructed sea ice concentration dataset [22], covering the period from 1901 to 2020 for all months. The ERSSTv5 observational dataset [23] was used for analyzing the SST data. SLP data were obtained from the HadSLP2 observational dataset [19].

3. Results

3.1. Extreme Hydrological Phenomena and Droughts on the East European Plain in 1920–1940

On the EEP, the ETCW was marked by an unprecedented rise and fall in the annual runoff of the Volga and Northern Dvina rivers in 1920–1940, recorded in the long-term hydrological time series, since 1882. An analysis of the SAT, precipitation anomalies and PDSI, based on observational data and 20th century re-analyses, proves the exceptionality of the 1920–1940 period and its association with large-scale extreme humidification anomalies of both signs (Figure 2a,b).

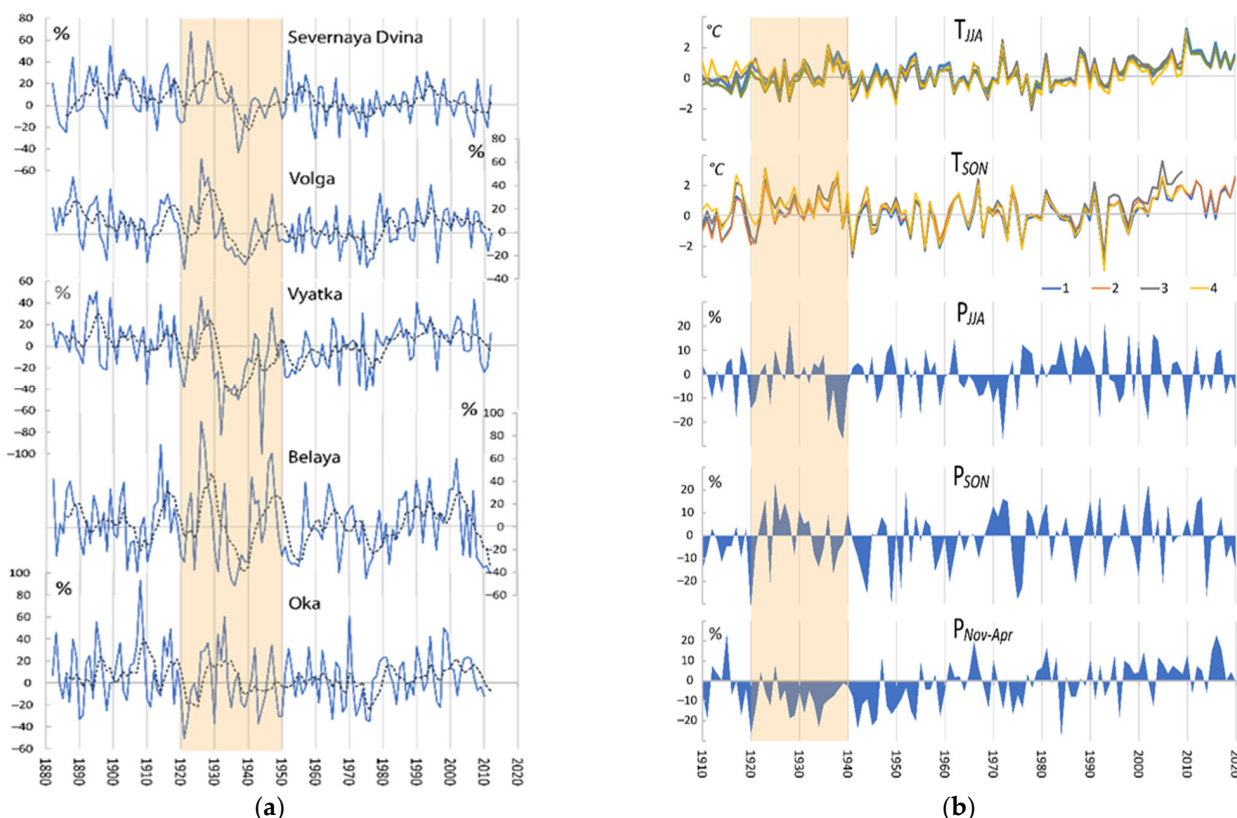


Figure 2. (a) Annual runoff, percent when compared with 1961–1990, for the rivers Severnaya Dvina, Volga, Vyatka, Belaya, and Oka; dotted line shows 5-year running averages. (b) Spatially averaged (20–60 E; 45–70 N) variations in the SAT anomalies, °C, 1, GISSTEMP, 2, CRUTEM, 3, ERA20C, 4, CERA20C, and precipitation; percent when compared with 1961–1990, for summer (JJA), autumn (SON), and cold period (November–April).

An abrupt fall in the water discharge in 1930 led to a 9-year period that saw the continuous deficit of annual Volga runoff (on average about 18%), which became the absolute maximum duration for the observation period; the next low-water period in 1954–1957 lasted for 4 years, with an 8% shortage in the runoff per year on average (Figure 2a). The anomalies in the annual runoff of the Northern Dvina, Vyatka and Belya rivers demonstrate a more significant amplitude, in contrast to the westerly located Oka basin, where the investigated phenomenon does not manifest itself. The latter probably indicates the southeast–northwest transport of the air masses responsible for the formation of drought.

Variations in the SAT and precipitation on the EEP for the 1910–1950 period demonstrate summer extremes of both signs; this includes cold and humid summers in 1923, 1926 and 1928, and prolonged drought against the background of abnormal heat in 1931 and 1936–1939. (Figure 2b). In addition to abnormally hot and dry summers, the most important role in the formation of droughts is assigned to the deficit of precipitation during the cold period, which lasted from the mid-1890s to the mid-1950s.

The average rate of the summer (JJA) temperature rise on the EEP for 20 years was 1.4 °C. The rates of this trend are inferior to the rates of modern summer warming since the early 1990s by 0.6 °C; however, as demonstrated by the PDSI changes, the growth rates of moisture deficiency and the duration of drought on the EEP (1934–1940) have no analogue during the observation period (Figure 3). The spatial distribution of the PDSI for the four driest years on average (Figure 3) demonstrates that, in a significant part of the EEP region, especially in the Volga and Northern Dvina supply source areas, i.e., in the Kama, Vychegda, and Upper and Middle Volga basins, the index values fall below −4 (locally below −5); this indicates an extreme drought according to the Palmer classification. Yet, an even more severe extreme drought, with sustained PDSI values below −5, was observed in the north-west of Kazakhstan.

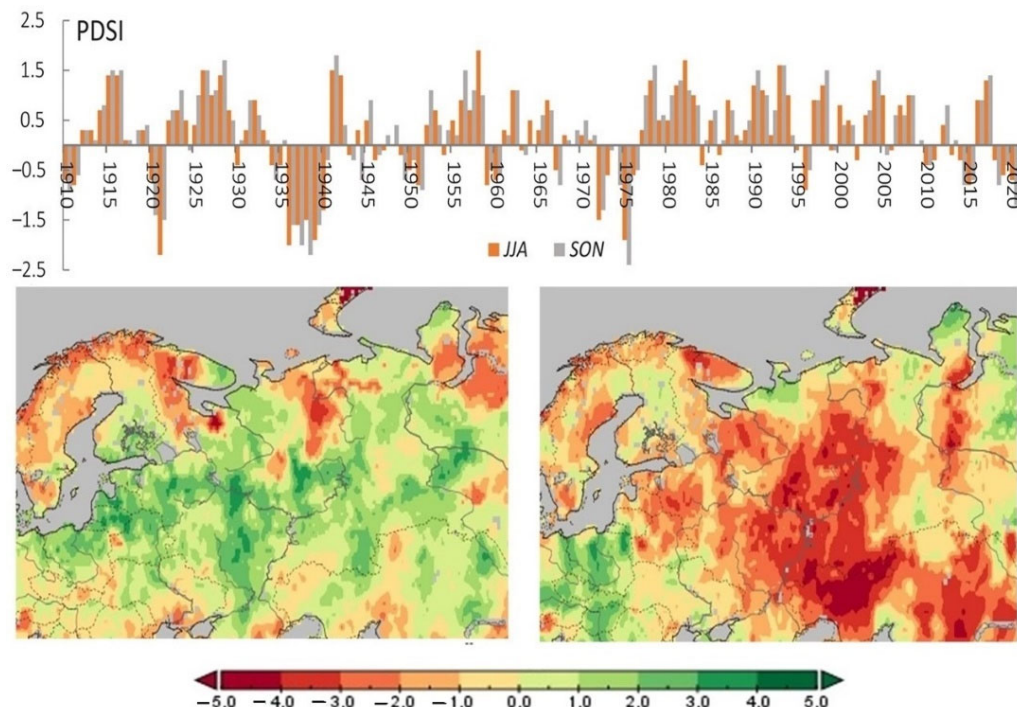


Figure 3. Spatially averaged (20–60 E; 45–70 N) PDSI, for JJA and SON seasons (upper panel) and spatial distribution of the JJA PDSI for “wet” (1923, 1926, 1927, 1928), (left bottom panel) and “dry” (1936, 1938, 1939, 1940) (right bottom panel) years.

3.2. Atmospheric Circulation Conditions and Drivers of Summer Warming and Extreme Drought on the EEP during the ETCW Period

The main difference in the distribution of SLP during abnormally hot summers (Figure 4a) on the EEP is associated with the subtropical high pressure belt, particularly with its significant increase in the Atlantic compared with the “cold” anomalies (Figure 4a); this belt spread to the north to the Arctic sector, and to the east, to beyond the Ural mountains. The noted features are clearly manifested in the SLP difference between the patterns that are referred to as the summer SAT anomalies of different signs (Figure 4a). Since a strong summer circulation on the EEP is established normally only from July, in this case, we consider the events of the SAT to be anomalous in July–August. Accordingly, average July–August SAT “hot” anomalies (above the standard deviation) were observed in 1931, 1936, 1938, and “cold” anomalies (below the standard deviation) were observed in 1923, 1926 and 1928.

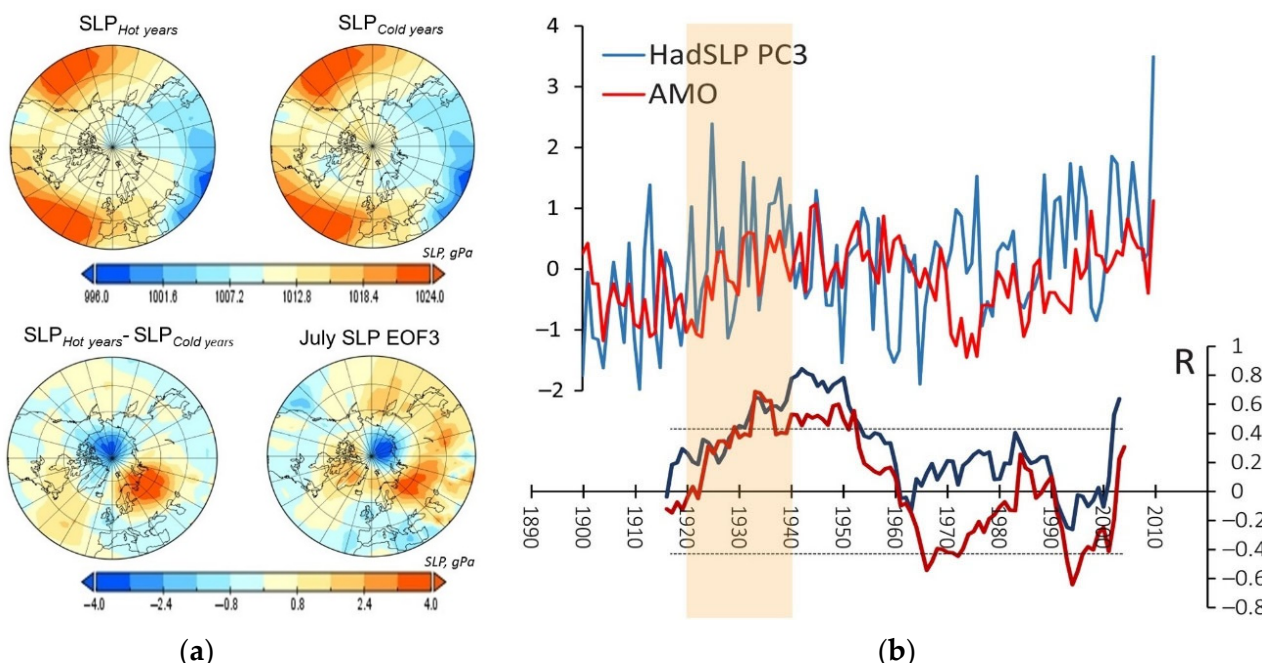


Figure 4. (a) Averaged SLP, gPa patterns for the years of “hot” (1931, 1936, 1938) and “cold” (1923, 1926, 1928) SAT anomalies on EEP; the difference between them and the EOF3 of SLP variability in July–August. (b) SLP PC3 and AMO($\times 4$) (upper panel) and correlation coefficients between (blue) SLP PC3 and July–August SAT anomalies on EEP, (red) AMO and SLP PC3, calculated over 15-year running periods; horizontal dotted lines indicate the threshold level of statistically significant values ($p < 0.05$).

The main anticyclonic center located over the north and northwest regions of the EEP borders, alongside a cyclonic anomaly with a center in the circumpolar region, can be characterized as a tripole; this, in turn, is blocked by an extensive anticyclonic anomaly to the south of Greenland. Considering the extensive anticyclonic pressure anomaly in the North Pacific Ocean, which indicates the “filling” of the Aleutian depression and the weakening of zonal circulation in the North Pacific Ocean sector, the distribution of pressure anomalies described above creates the conditions for the formulation of the blocking anticyclone over the EEP; this increases the warm and dry air flow from the subtropics to mid and high latitudes, up to the Barents and Kara Seas. This scheme may be regarded as the direct mechanism of the formation of heat and drought in the considered time period.

An EOF analysis of the SLP variability in the Northern Hemisphere (NH) extratropical zone in the July–August summer months (JA) for 1900–2010 shows that the SLP anomalies

in the second half of the 1930s and 2000s are described by the 3rd spatial structure of EOF3 (in accordance with the explained variance of 13%) and the corresponding PC3 (Figure 4a,b). The main features of EOF3 (Figure 4a) are an extensive anticyclonic anomaly centered on the EEP and a cyclonic anomaly in the circumpolar region of the Eurasian sector, as well as a high pressure belt extending eastward through Asia to the Pacific Ocean, and westward to the Atlantic and American sectors of the Arctic Ocean. A temporal variation in the PC3 (Figure 4b) in 1900–2010 demonstrates the long-term fluctuations, with two positive phases corresponding to the summer temperature anomalies during ETCW and the late 1990s–2000s, with an absolute maximum in 2010 also.

The linear correlation between the SLP PC3 and the JA-averaged SAT for the EEP, calculated from 15-year running periods (Figure 4b), demonstrates two statistically significant ($p > 0.05$) maximums; one is during the ETCW, up to 0.6–0.8 in 1930–1950, and the other is in the last 15 years, with 0.5–0.6. The relatively high correlation indicates that the pattern of the obtained EOF3 explains the circulation mechanism of the SAT anomalies on the EEP during the ETCW and during the period of modern warming. A similar correlation of PC3 with the AMO is found for the ETCW (Figure 4b), in addition to the noted correlation of SLP PC3 with the July–August SAT. The values of the correlation coefficients reach statistical significance in the 1930s and 1950s, decrease to statistically insignificant values after the 1950s, change in the sign in the 1960s, 1980s and 1990s, and reach statistically significant values in the 2000s. In contrast to the interannual variations in the link between PC3 and the AMO, long term fluctuations seem to be stable for the 1900–2010 period.

At the same time, the correlation coefficient between July's spatially averaged SAT on the EEP and the AMO index (Figure 5a) during ETCW turns out to be statistically significant only for a 15-year period, in 1926–1940.

During the 1923–1950 period (Table 1), there is a statistically insignificant value ($p < 0.05$). A sustainable link between these parameters, with a correlation coefficient of 0.61, is marked in 1980–2000 during the period of positive AMO after the index minimum in the 1970s (Figure 5a, Table 1).

Table 1. Correlation of AMO, SST_{S1} and ΔSST_{S1-S2} (March–April) with SAT_{EEP} , July, and Barents Sea ice area, May *.

Parameter	Years	AMO	SST_{S1}	ΔSST_{S1-S2}
AMO	1910–2020	-	0.68	0.36
SAT_{EEP}	1923–1950	0.27	0.53	0.59
SAT_{EEP}	1980–2000	0.61	0.50	0.41
BS ice area	1923–1940	−0.25	−0.48	−0.34

* The time series used were detrended for the above periods; statistically significant ($p < 0.05$) correlation coefficients are marked by bold.

The analysis of the NA SST indicates an inhomogeneity in the spatial distribution of SST anomalies in the period of ETCW in the years of the considered SAT anomalies on the EEP, “hot” (1931, 1936, 1938) and “cold” (1923, 1926, 1928). The difference in the SST between the averages of the “hot” and “cold” anomalies for these years (Figure 5b) demonstrates two zones of positive anomalies; one is in the northwest, along the 40–55 N latitudes, and the other is in the tropical zone of the NA, divided by the belt of the opposite sign anomalies with a maximum northward of the Greater Antilles. The noted spatial pattern manifests itself already in the winter season, but the maximum values of anomalies are reached in March–April. The closest relation between the NA SST and the July SAT on the EEP during the ETCW are observed in the same months (Figure 5b). It should be noted that the spatial distribution of the centers of correlation, which are positive in the northwest of the NA (S1—20–50 W, 40–50 N) and negative northward of the Greater Antilles (S2—65–80 W, 20–30 N), corresponds to the pattern of SST anomalies considered above (Figure 5b).

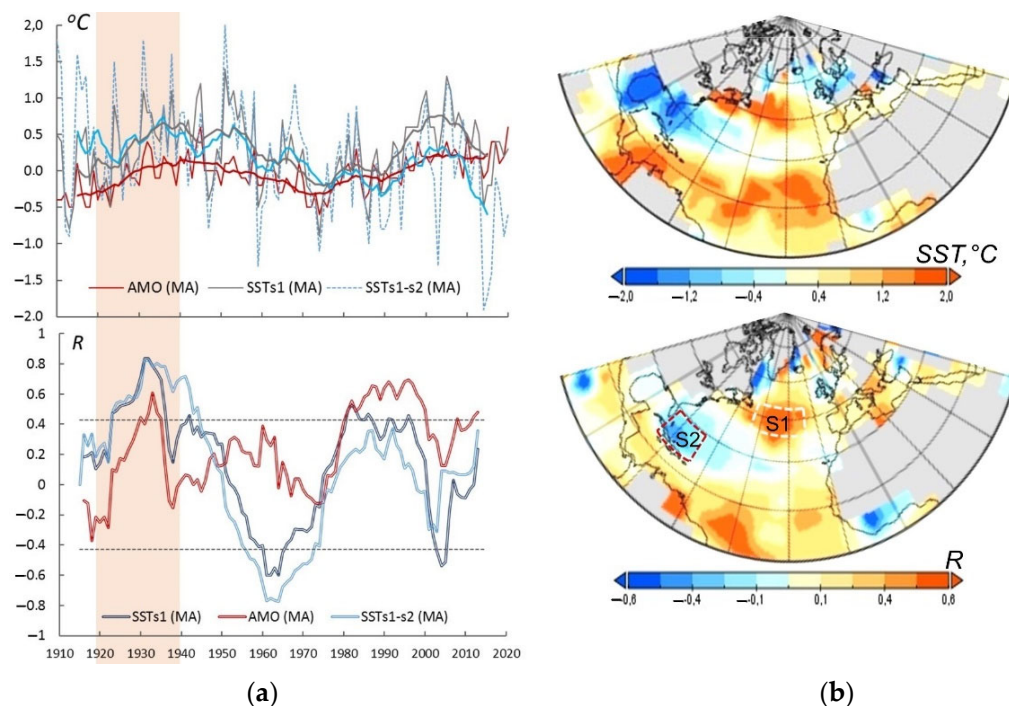


Figure 5. (a) Variation in the AMO, SST anomalies, $^{\circ}\text{C}$, averaged in sector S1 (20–50 W, 40–50 N), $\text{SST}_{\text{S}1}$, and SST difference, $^{\circ}\text{C}$, between S1 and S2 (65–80 W, 20–30 N), $\Delta\text{SST}_{\text{S}1-\text{S}2}$, March–April (upper panel); thin (thick) lines show annual values (15-year running averages). Correlation coefficients between July SAT on the EEP (20–60 E; 45–70 N) and detrended timeseries of AMO, $\text{SST}_{\text{S}1}$, $\Delta\text{SST}_{\text{S}1-\text{S}2}$ (March–April), calculated over 15-year running periods (bottom panel); horizontal dotted lines indicate the threshold level of statistically significant values ($p < 0.05$). (b) Difference between SST, $^{\circ}\text{C}$, (March–April) averaged for the years of “hot” (1931, 1936, 1938) and “cold” (1923, 1926, 1928) July SAT anomalies on the EEP (upper panel), and correlation between SST and July SAT on the EEP, detrended, in 1923–1950; white and red dashed lines indicate the borders of S1 and S2, respectively (bottom panel).

Comparison of a long-term timeseries of the $\text{SST}_{\text{S}1}$ variation, averaged for the selected sector in the northwest of the NA (Figure 5a) with the AMO index, and averaged for March–April, indicates differences in interannual variability, as well as the absence of the trend for 1910–2020; this is unlike AMO with the linear trend, which accounts for almost 15% of the total variability. The correlation of the detrended time series of the July SAT on the EEP and $\text{SST}_{\text{S}1}$, which is 0.53 ($p < 0.05$) for 1923–1950 (Table 1) on a 15-year running period (Figure 5b), also distinguishes $\text{SST}_{\text{S}1}$ long-term variability from AMO. The variation in the 15-year running correlation coefficients between the July temperature on the EEP with $\text{SST}_{\text{S}1}$ in 1910–2020 differs from similar estimates for the AMO; there is a sharp decrease from the 1950s, and a transition to the opposite sign values from the late 1950s to the 1970s by a general downward trend. Despite the simultaneous increase in the correlation coefficients in 1980–2000, in the case of $\text{SST}_{\text{S}1}$, it remains close to the coefficient values of 1923–1950; the correlation coefficient was 0.50 for 1980–2000. This is unlike the AMO, which saw a significantly increased correlation up to 0.61, compared to 1923–1950 (Table 1, Figure 5b). This estimate indicates the probable impact of $\text{SST}_{\text{S}1}$ anomalies as a driver of summer SAT anomalies on the EEP, and also the features of their long-term variability, different from the AMO.

Considering the $\text{SST}_{\text{S}2}$, the anomalies of the opposite sign in the sector S2, northward of the Greater Antilles (Figure 5b), the long-term variability in the difference between the $\text{SST}_{\text{S}1}$ and $\text{SST}_{\text{S}2}$ anomalies was analyzed. The resulting time series $\Delta\text{SST}_{\text{S}1-\text{S}2}$ (Figure 5a) shows more significant discrepancies with the AMO, comparative to the $\text{SST}_{\text{S}1}$. Foremost, it is the significant downward trend in the $\Delta\text{SST}_{\text{S}1-\text{S}2}$ that accounts for 44% of its total

variability in 1910–2020, which obviously reflects the differences in the rates of SST increase between the north-west of the NA in the S1 sector, and the west of the tropical zone of the NA in the S2 sector. The correlation between the long-term (1910–2020) time series of $\Delta\text{SST}_{\text{S1-S2}}$ and the AMO is 0.36, which is significantly lower compared to SST_{S1} and accounts for 0.68 (Table 1). The 15-year running correlation between $\Delta\text{SST}_{\text{S1-S2}}$ and the July SAT on the EEP demonstrates that there was a stable relationship from the beginning of 1920 to the middle of 1940 and its weakening in 1980–2000 (Figure 5a, Table 1). The 1923–1950 correlation coefficient accounts for 0.59, and in 1980–2000, it decreases to 0.41. Apparently, the noted features of the $\Delta\text{SST}_{\text{S1-S2}}$ time series mean are that the ETCW July SAT anomalies on the EEP are related not only to the warming of the NA, but also with the certain spatial pattern of SST anomalies characteristic of the 1920–1950 period (Figure 5a). The transition of the correlation coefficient values between $\Delta\text{SST}_{\text{S1-S2}}$ and the July SAT on the EEP into the opposite sign from the mid-1950s to the mid-1970s is a matter of interest in terms of changes in the mechanisms of SAT anomaly occurrence in these years (please note that the temperature extreme observed on the EEP in 1972 is second in magnitude only to the absolute maximum of 2010), but goes beyond the scope of this study.

Comparing the cases of the AMO and $\Delta\text{SST}_{\text{S1-S2}}$, the distribution of the regression coefficients of the NA SST in early spring (March–April) onto the SLP of the NH extratropical zone in 1920–1950 demonstrates the different degrees of their impact (Figure 6) and significant spatial differences.

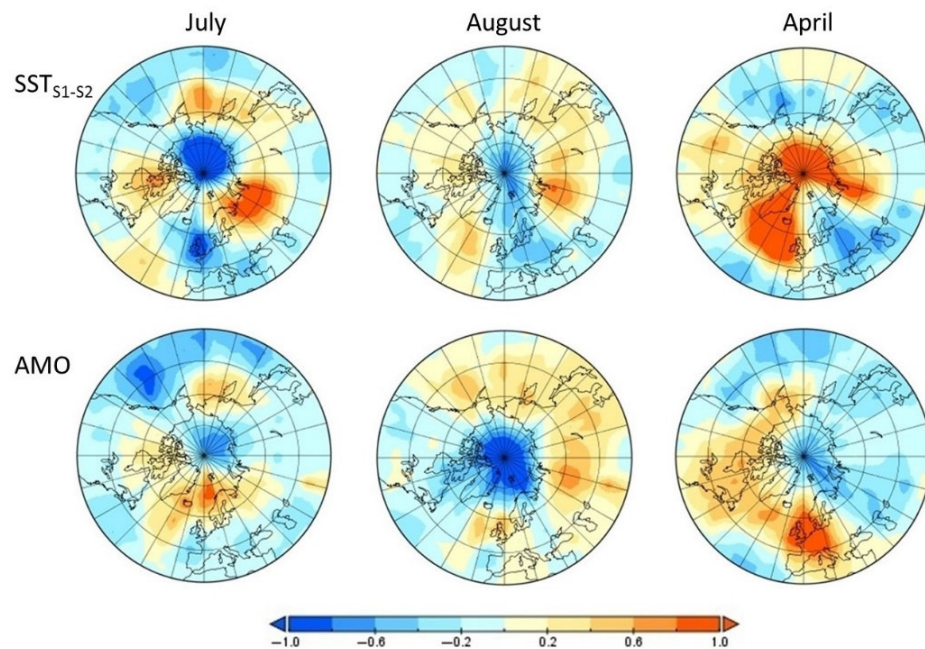


Figure 6. Linear regression coefficients of timeseries of AMO and $\Delta\text{SST}_{\text{S1-S2}}$ (March–April), detrended and normalized onto SLP anomalies: July, August, April, in 1923–1950.

Foremost, this refers to the SLP field in July (Figure 6). The main centers of the regression field, $\Delta\text{SST}_{\text{S1-S2}}$, represent a dipole: there is a positive anomaly extending to the EEP and the adjacent territories beyond the Urals, and a vast negative anomaly in the circumpolar region. Small centers in the east Atlantic mid latitudes and in the north of the Pacific Ocean are also quite noticeable. The center of the positive regression of $\Delta\text{SST}_{\text{S1-S2}}$ on the SLP located beyond the Urals persists in August and is similar to that observed in July, but weaker. In general, this corresponds to the SLP difference patterns in the years of “hot” and “cold” SAT anomalies on the EEP, as well as the pattern of EOF3 of SLP variability in 1910–2010 (Figure 4a).

The AMO regression on the SLP in July is significantly weaker, although the spatial distribution of the positive regression areas, including the EEP and the adjacent region

beyond the Urals, demonstrates similarities with the $\Delta\text{SST}_{\text{S1-S2}}$ (Figure 6). A small positive center is observed in the east of the Arctic sector of the Atlantic, which is negative in the east of the Pacific Ocean and in the circumpolar region of the East-Eurasian sector. In August, unlike July, the AMO regression on the SLP field shows a very similar pattern to $\Delta\text{SST}_{\text{S1-S2}}$, with a maximum beyond the Urals; however, this differs with more significant negative regression coefficients in the circumpolar region.

The most pronounced discrepancies between the fields of the regression coefficients of the AMO and $\Delta\text{SST}_{\text{S1-S2}}$ on the SLP are marked in April (Figure 6). However, in both cases, the distribution and intensity of the maximum coefficients indicate their relationship with the formation of extensive anticyclones, contributing to the strengthening of inter-latitude exchange and the transfer of warm air masses from low latitudes to the Arctic. In the case of $\Delta\text{SST}_{\text{S1-S2}}$, an anticyclone in Western Siberia that is associated with the NA SST anomalies and is expressed by $\Delta\text{SST}_{\text{S1-S2}}$ forms conditions that enable warm air to flow from low latitudes along its western periphery to the Barents–Kara Sea area. The abnormal spring warming caused by such circulation anomalies can contribute to the earlier loss of the sea ice [24,25] and, additionally to the warm Atlantic waters inflow; this results in delayed cumulative effects and leads to a reduction in the SIE. Anomalies in the sea ice area in the Barents Sea in May in 1923, 1926, 1928, 1931 and 1936 (Figure 7a) coincide with the July SAT anomalies on the EEP and probably reflect the contribution of the NA SST anomalies. At the same time, there is no obvious evidence of the influence of $\Delta\text{SST}_{\text{S1-S2}}$, as the correlation of the sea ice area in the Barents Sea in May is revealed only for SST_{S1} in a short period in 1923–1940 (Table 1).

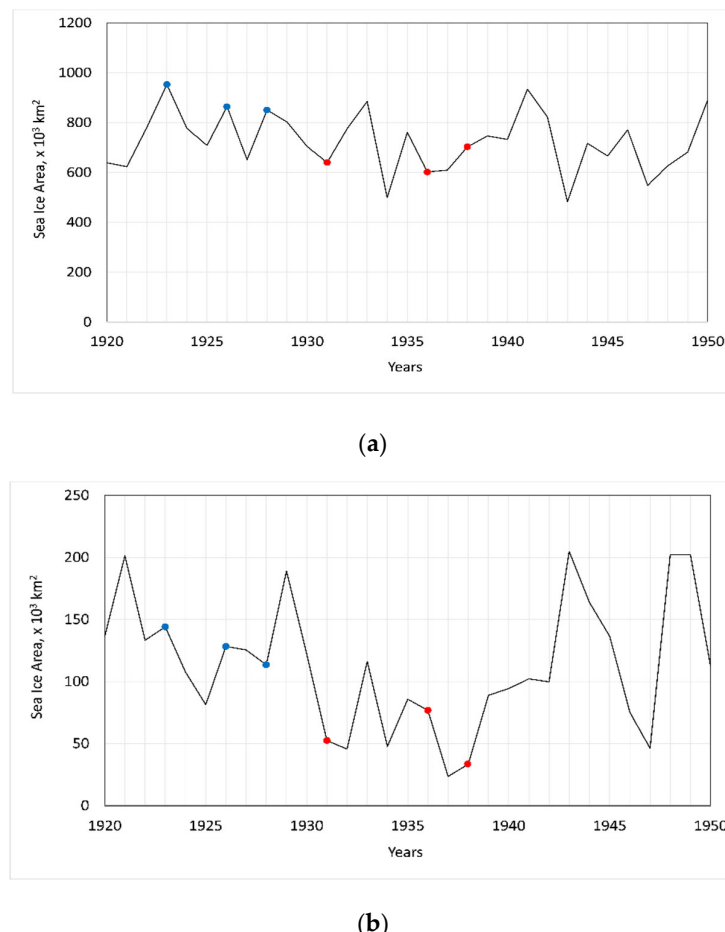


Figure 7. Sea ice area ($\times 10^3 \text{ km}^2$) in the Barents Sea in (a) May and (b) August; Blue (red) dots indicate years of positive, red, and negative, blue, July SAT anomalies on the EEP.

3.3. The Link of Summer Warming and EEP Drought in 1920–1940 to Arctic Warming and Changes of Sea Ice Area in the Barents and Kara Seas

Comparison of the SIE in June and August in the Barents Sea during the years of positive and negative SAT anomalies on the EEP demonstrates a significant decline in the sea ice area in August within years of positive anomalies, compared to the years of negative anomalies (Figure 7).

The analysis of the spatial patterns of SIC in the years of positive and negative temperature anomalies on the EEP suggests that there are spatial features. May and August were analyzed as a month of sea ice melt onset and as a month of SIE minimum, respectively. In May, the SIC increased northeastward to the Novaya Zemlya archipelago in the years of negative temperature anomaly compared to positive ones, demonstrating the greatest difference between the considered cases (Figure 8a). In August, an increase (decrease) in the SIC in the years of negative (positive) temperature anomaly was observed in the north part of both the Barents and Kara Sea (Figure 8b). The spatial features of the SIC differences indicate the influence of the warm Atlantic water inflow variability to the Barents–Kara Sea.

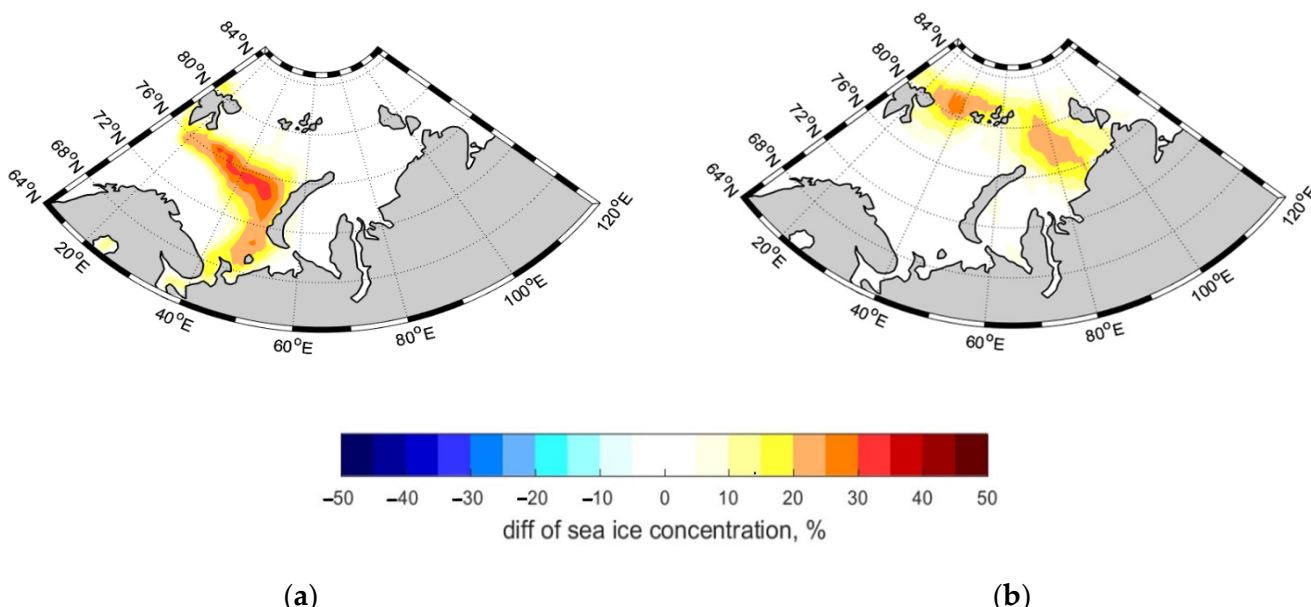


Figure 8. Difference in SIC (%) between the years of negative and positive July SAT anomalies on the EEP in (a) May and (b) August.

The AMO can also affect the SIE in the Barents–Kara Sea region. Meanwhile, sea ice decline in the Barents Sea in spring can lead to a formation of a cyclonic vortex over the Barents Sea (Figure 9). This atmosphere circulation response, in turn, can increase the oceanic in-flow of warm and salty Atlantic water masses. This positive feedback causes further sea ice loss. Moreover, warmer Barents and Kara Seas may result in atmospheric blocking conditions south of the Barents Sea, and may contribute to a precipitation deficiency and a positive SAT anomaly on the EEP.

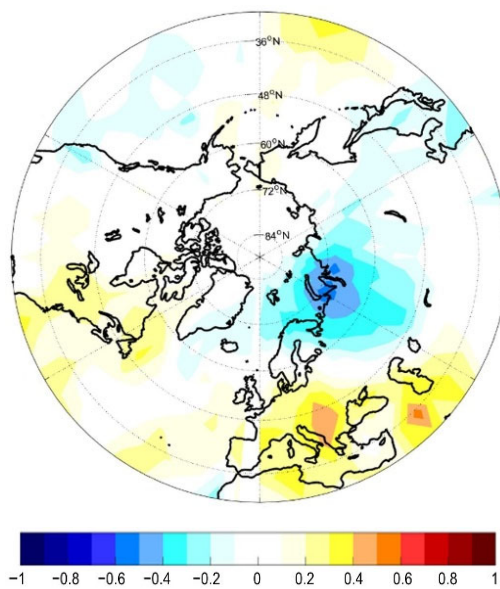


Figure 9. Correlation coefficients between SIA in the Barents Sea in May and SLP anomalies in July for 1924–1950.

4. Discussion

The analysis of climate characteristics and the aridity index on the EEP for 1910–2020 demonstrates that the ETCW period, in particular 1920–1940, was marked by a strong long-term drought that followed a short period of increased humidification. In the catalogue of severe droughts on the EEP [26], the 1930s, as well as the 1950s and the 1990s, are characterized by a high frequency of drought occurrence. At the same time, the droughts recorded during the investigated period (1931, 1936, 1938, 1939) were not considered as events distinct from 32 other severe droughts observed on the EEP in 1891–2010, which were not studied in the context of the ETCW as well. The results of our analysis show that the precipitation deficit, as well as the intensity and duration of recurrent drought in 1934–1940, have no analogues during the observation period.

Equivalent phenomenon outside of Northern Eurasia at lower geographical latitudes during the ETCW period, in particular catastrophic droughts in the 1930s on the Great Plains, North America, have been previously studied [3,5–8]. In the context of circulation conditions, these phenomena are associated with the northward expansion of the Hadley cell and the subtropical high pressure belt [3,9]. The patterns of atmospheric pressure anomalies, identified by EOF analysis, as well as obtained by studying SLP anomalies during the years of severe droughts of the 1930s, also indicate similar events. The expansion of the subtropical high-pressure belt over the Atlantic is able to affect planetary atmospheric waves in mid-latitudes and, apparently, become one of the main forces behind a strong sustainable anticyclone over the center of the EEP. In combination with a cyclonic anomaly in the circumpolar region, this forms a dipole pattern that is typical of the circulation conditions of the dry and hot summers of the 1930s and has close similarity with the previously described circulation mechanism of Arctic warming during the ETCW [27]. The considered atmospheric pattern can be related to the Arctic Sea ice changes, particularly in the Barents and Kara Sea region. The relationship between sea ice variability in the region and the atmospheric circulation patterns (both for the recent and early warming periods) was described in [28,29] but still requires clarification of its connection to droughts in the 1930s on the EEP.

The duration of the summer SAT anomalies and moisture deficiency period, which covers the second half of the 1930s, indicates the presence of large-scale factors. Such factors include the NA SST anomalies, which are expressed by the AMO index and have low-frequency fluctuations with a period of approximately 60–80 years. According to

the results of numerous studies, including those that use numerical simulation [2], the NA SST rise pronounced by the positive phase of the AMO observed in the 1930–1940s could have caused the climate changes recorded during the ETCW period. The obtained estimates [30] indicate that the AMO has a leading contribution to the variability in the NH SAT by up to 80%. Our analysis of the long-term (1900–2010) variations in the SLP EOF3 mode, describing the mechanism of hot and dry summer circulation on the EEP, indicates a connection with the AMO [3], in particular, its positive phases in the 1930s–1940s and in the 2000s.

Considering the impact of the NA region on the temperature regime of Europe spreading eastward up to Central Siberia [31], the positive phase of the AMO is obviously the most important factor that contributes to the summer SAT anomalies on the EEP. Research results [30] lead to the conclusion that the NA warming crucially contributes to the ETCW phenomenon.

This study did not reveal a statistically significant correlation between the AMO and the July SAT on the EEP during the ETCW. The analysis of SST anomalies demonstrates that the warming of the NA SST during this period was meridionally inhomogeneous. The spatial distribution of SST anomalies within the years of “hot” anomalies is characterized by two zones of positive anomalies: one is in the northwest along the 40–55 N latitudes, and the other is in the tropical belt of the NA, divided by the belt of anomalies of the opposite sign with a maximum on the west of the NA subtropical zone, northward of the Greater Antilles. According to [31], such a pattern is associated with the negative phase of the North Atlantic Oscillation, which is characterized by a weakening of zonal transport over the NA and the Atlantic sector of Northern Eurasia. A similar pattern is detected in the spatial distribution of the correlation between SST and the July SAT on the EEP with two centers: one is positive, in the northwest of NA (S1), and the other is negative, northward of the Greater Antilles (S2). The importance of regional SST changes for the regional and Arctic climate was emphasized in [31]; it was noted that the early 20th-century Arctic warming is also associated with positive SST anomalies over the tropical and North Atlantic, and with a Pacific SST pattern that is reminiscent of the positive phase of the Pacific Decadal Oscillation.

A comparative analysis of the long-term timeseries (1910–2020) of the AMO and SST anomalies, averaged in the centers of the maximum correlation, shows that they are positive in the northwest of the NA and are negative in the west of the NA subtropical zone; SST_{S1} and ΔSST_{S1-S2} show the differences in the latter from the AMO. The features of the long-term changes in ΔSST_{S1-S2} refer to a stable relationship between the July SAT on the EEP during the period of the ETCW (1923–1950) and its weakening in the modern period (1980–2000) against the background of a downward trend for 1910–2020. This distinguishes ΔSST_{S1-S2} from AMO, whose long-term course is characterized by a trend corresponding to modern warming and a fairly high correlation with the July SAT on the EEP in 1980–2000. The noted features of the ΔSST_{S1-S2} time-series indicate that the ETCW July SAT anomalies on the EEP are related not only to the NA warming, but also to a certain spatial pattern of SST anomalies in the 1920–1950 period.

The spatial distribution of regression of ΔSST_{S1-S2} and the AMO on the SLP field during ETCW confirms this conclusion. In case of ΔSST_{S1-S2} , it demonstrates a distinct dipole pattern revealed in the SLP anomaly field for the years of “hot” SAT anomalies on the EEP, with an anticyclonic center on the EEP and the adjacent region beyond the Ural Mountains, and a cyclonic center over the circumpolar region. Unlike ΔSST_{S1-S2} , the AMO regression shows a similar structure only for the SLP in August; however, this is less intense in the centers.

The long-term timeseries of ΔSST_{S1-S2} , which demonstrates the downward trend, could be considered to be indicative of the changes in the role of the pattern described above and how it affects the NA SST variability of the 1910–2020 period; it is also an indicator of its weakening in the modern period.

The variability in the sea ice area of the Barents Sea in May coincides with the July SAT anomalies on the EEP and probably reflects the contribution of the NA SST anomalies. However, there is no obvious evidence of the impact of ΔSST_{S1-S2} , as the correlation of the sea ice area in the Barents Sea in May is revealed only for ΔSST_{S1} in a short period in 1923–1940 at the beginning of ETCW.

The growth of summer temperature extremes on the EEP is observed in the period of modern warming (Figure 2b). After the considered events of the 1930s, extreme heat and drought events were observed in 1972 and 2010. The flow fall of the Volga river (Figure 1) and the level of the Caspian Sea in the early 1970s, which followed a long-term rainfall deficit in the late 1960s (Figures 2b and 3) and droughts in 1972 and 1975 [26]), could be partially associated with increased anthropogenic impact, in particular, with the use of runoff for the irrigation of agricultural areas. The Northern Dvina runoff also noticeably decreased in these years (Figure 2). Since the 1980s–1990s, the rate of summer temperature growth on the EEP has increased significantly; 2010 was marked by the absolute maximum temperature over the observation period and is known for catastrophic consequences for the natural environment and society. As our estimates show, the NA warming contributes to this trend in 1980–2000 (Figure 4a). The influence of the Pacific Ocean increases significantly in the 1990–2000s according to a number of studies, which assign it a decisive role in the 2010 event [32,33].

Simultaneously, the river runoff response to these events is not comparable to the period of the 1930s (Figure 2). First of all, this is due to the natural increase in precipitation under modern climate warming [34], especially noticeable during the cold period (Figure 1b), which compensates for evaporation losses against the background of rising summer temperatures (Figures 2b and 3). A certain role in the smoothing of Volga runoff response may belong to the anthropogenic overregulation of its river system. Thus, the evaporation increase from river catchments is offset by an increase in precipitation, although, according to the water balance component forecasts made on the basis of CMIP5 [35], its ratio may change towards the growth of evaporation in the second half of the XXI century.

5. Conclusions

The study of climatic characteristics and the annual runoff of the Volga and Severnaya Dvina rivers shows that, on the EEP, the ETCW manifested in a multiyear drought in 1934–1940 that caused extreme hydrological events and that, according to Palmer's classification, has no analogues in this region in intensity and duration. The circulation conditions during this event are characterized by an extensive anticyclone over Eastern Europe, combined with a cyclonic anomaly in the circumpolar region.

We examined the relationship between SAT extremes on the EEP and North Atlantic SST anomalies, with focus on their spatial distribution. The analysis allowed us to obtain new results that highlighted the global- and regional-scale factors contributing to the formation of summer temperature anomalies and extreme droughts in the 1930s on the EEP. The spatial distribution of the SST anomalies within the years of “hot” and “cold” SAT anomalies on the EEP is meridionally inhomogeneous, and reveals two zones of positive and negative anomalies: one is in the northwest along the 40–55 N latitudes, and the other is in the tropical belt of the NA, divided by the belt of anomalies of the opposite sign with a maximum on the west of the NA subtropical zone.

Time series of the difference between the SST in the NA anomaly zones of opposite signs, used as an indicator of the resulting spatial pattern of the SST, shows a fairly close and stable relationship with the July SAT anomalies on the EEP and the atmospheric circulation patterns responsible for them in 1920–1950. In contrast, the AMO demonstrates a statistically insignificant correlation in 1920–1950 and a high correlation with the July SAT anomalies on the EEP in 1980–2000.

Thus, the analysis of the temporal features of the SST anomalies shows that the July SAT anomalies, and summer heat and drought events on the EEP are associated not only with the warming of the NA and the positive phase of the AMO, but to a greater degree

with a certain spatial pattern observed in the spring SST anomalies of 1920–1950. In long-term variation, the revealed indicator of this spatial pattern demonstrates that there has been a downward trend since the 1960s and that its links with the summer SAT on the EEP in the modern period have weakened.

The positive AMO phase and the expansion of the subtropical high-pressure belt to the north and to the east can be considered as global-scale drivers of this phenomenon. The AMO also impacts the sea ice cover in the Barents–Kara Sea region and, in turn, could have led to specific atmospheric circulation patterns and contributed to the drought events on the EEP in the 1930s.

Author Contributions: Conceptualization, V.P.; methodology, V.P. and T.A.; validation, formal analysis and investigation, V.P., T.A. and D.B.; resources and data curation, V.P., T.A. and D.B.; writing and editing, V.P., T.A. and D.B.; visualization V.P. and T.A.; supervision and project administration, V.P. All authors have read and agreed to the published version of the manuscript.

Funding: This research was funded by Russian Science Foundation (RSF) grant number 22-27-00495.

Data Availability Statement: The study is based on the publicly archived datasets and generated during the previous investigations: SAT gridded datasets include observational data, HadCRUT5 (<https://crudata.uea.ac.uk/cru/data/temperature/>, accessed on 1 July 2022), GISSTEMP (v4 <https://data.giss.nasa.gov/gistemp/>), and 20th century re-analysis, ERA20C (<https://apps.ecmwf.int/datasets/data/era20c>), CERA-20C (<https://apps.ecmwf.int/datasets/data/cera20c>); precipitation data and Self-calibrating Palmer Drought Severity Index—CRU TS v4.05 (https://crudata.uea.ac.uk/cru/data/hrg/cru_ts_4.05/), scPDSI (<https://crudata.uea.ac.uk/cru/data/drought/>); Sea Level Pressure—HadSLP2 (<https://www.metoffice.gov.uk/hadobs/hadslp2>); AMO—NOAA PSL1 (<http://www.psl.noaa.gov/data/timeseries/AMO/>); Sea Surface Temperature—HadSST.4.0.0.0 (<https://www.metoffice.gov.uk/hadobs/hadsst4/>). Data on the SIE in August for the Kara Sea from 1924 was obtained from the Arctic and Antarctic Research Institute database (<https://nsidc.org/data/g02182 VERSIONS/1>, free access). For the Barents Sea, the new reconstructed SIC data set was used (data can be sent upon request to Tatiana Aldonina (Matveeva) (matveeva.tatiana@igras.ru)).

Conflicts of Interest: The authors declare no conflict of interest.

References

1. Bokuchava, D.; Semenov, V. Mechanisms of the Early 20th Century Warming in the Arctic. *Earth-Sci. Rev.* **2021**, *222*, 103820. [[CrossRef](#)]
2. Chylek, P.; Klett, J.D.; Dubey, M.K.; Hengartner, N. The role of Atlantic Multi-decadal Oscillation in the global mean temperature variability. *Clim. Dyn.* **2016**, *47*, 3271–3279. [[CrossRef](#)]
3. Hegerl, G.C.; Brönnimann, S.; Schurer, A.; Cowan, T. The early 20th century warming: Anomalies, causes, and consequences. *WIREs Clim. Chang.* **2018**, *9*, e522. [[CrossRef](#)]
4. Brönnimann, S.; Stickler, A.; Griesser, T.; Ewen, T.; Grant, A.N.; Fischer, A.M.; Ross, T. Exceptional atmospheric circulation during the “Dust Bowl”. *Geophys. Res. Lett.* **2009**, *36*, L08802. [[CrossRef](#)]
5. Cook, B.I.; Seager, R.; Miller, R.L. Atmospheric circulation anomalies during two persistent north american droughts: 1932–1939 and 1948–1957. *Clim. Dyn.* **2011**, *36*, 2339–2355. [[CrossRef](#)]
6. Cowan, T.; Hegerl, G.C.; Schurer, A.; Tett, S.F.B.; Vautard, R.; Yiou, P.; Jézéquel, A.; Otto, F.E.L.; Harrington, L.J.; Ng, B. Ocean and land forcing of the record-breaking Dust Bowl heatwaves across central United States. *Nat. Commun.* **2020**, *11*, 2870. [[CrossRef](#)]
7. Schubert, S.D.; Suarez, M.J.; Pegion, P.J.; Koster, R.D.; Bacmeister, J.T. Causes of long-term drought in the U.S. Great Plains. *J. Clim.* **2004**, *17*, 485–503. [[CrossRef](#)]
8. Cook, B.I.; Miller, R.L.; Seager, R. Amplification of the North American “Dust Bowl” drought through human-induced land degradation. *Proc. Natl. Acad. Sci. USA* **2009**, *106*, 4997–5001. [[CrossRef](#)]
9. Brönnimann, S. Climatic changes since 1700. In *Advances in Global Change Research*; Springer: Berlin/Heidelberg, Germany, 2015; Volume 55, p. 360.
10. Brönnimann, S.; Fischer, A.M.; Rozanov, E.; Poli, P.; Compo, G.P.; Sardeshmukh, P.D. Southward shift of the northern tropical belt from 1945 to 1980. *Nat. Geosci.* **2015**, *8*, 969–974. [[CrossRef](#)]
11. Barry, J.M. *Rising Tide: The Great Mississippi Flood of 1927 and How it Changed America*; Simon & Schuster: New York, NY, USA, 1997; p. 526.
12. Wegmann, M.; Orsolini, Y.; Zolina, O. Warm Arctic–cold Siberia: Comparing the recent and the early 20th-century Arctic warmings. *Environ. Res. Lett.* **2018**, *13*, 025009. [[CrossRef](#)]

13. Wegmann, M.; Rohrer, M.; Santolaria-Otín, M.; Lohmann, G. Eurasian autumn snow link to winter North Atlantic Oscillation is strongest for Arctic warming periods. *Earth Syst. Dynam.* **2020**, *11*, 509–524. [[CrossRef](#)]
14. Popova, V.; Matveeva, T.; Bokuchava, D. The Early 20th Century Warming in the East-European Plain Climate: Extreme Drought in 1920–1940, Atmospheric Circulation Anomalies and Links with the Sea Ice Variability. *Environ. Sci. Proc.* **2022**, *19*, 57.
15. Morice, C.P.; Kennedy, J.J.; Rayner, N.A.; Winn, J.P.; Hogan, E.; Killick, R.E.; Dunn, R.J.H.; Osborn, T.J.; Jones, P.D.; Simpson, I.R. An updated assessment of near-surface temperature change from 1850: The HadCRUT5 dataset. *J. Geophys. Res.* **2021**, *126*. [[CrossRef](#)]
16. Lenssen, N.; Schmidt, G.; Hansen, J.; Menne, M.; Persin, A.; Ruedy, R.; Zyss, D. Improvements in the GISTEMP uncertainty model. *J. Geophys. Res. Atmos.* **2019**, *124*, 6307–6326. [[CrossRef](#)]
17. Harris, I.; Osborn, T.J.; Jones, P.; Lister, D. Version 4 of the CRU TS monthly high-resolution gridded multivariate climate dataset. *Sci. Data* **2020**, *7*, 56. [[CrossRef](#)] [[PubMed](#)]
18. Schrier, G.; Barichivich, J.; Briffa, K.R.; Jones, P.D. A scPDSI-based global data set of dry and wet spells for 1901–2009. *J. Geophys. Res. Atmos.* **2013**, *118*, 4025–4048. [[CrossRef](#)]
19. Allan, R.; Ansell, T. A New Globally Complete Monthly Historical Gridded Mean Sea Level Pressure Dataset (HadSLP2): 1850–2004. *J. Clim.* **2006**, *19*, 5816–5842. [[CrossRef](#)]
20. Kennedy, J.J.; Rayner, N.A.; Atkinson, C.P.; Killick, R.E. An Ensemble Data Set of Sea Surface Temperature Change From 1850: The Met Office Hadley Centre HadSST.4.0.0.0 Data Set. *J. Geophys. Res. Atmos.* **2019**, *124*, 7719–7763. [[CrossRef](#)]
21. Polyakov, I.V.; Alekseev, G.V.; Bekryaev, R.V.; Bhatt, U.S.; Colony, R.; Johnson, M.A.; Karklin, V.P.; Walsh, D.; Yulin, A.V. Long-Term Ice Variability in Arctic Marginal Seas. *J. Clim.* **2003**, *16*, 2078–2085. [[CrossRef](#)]
22. Semenov, V.A.; Matveeva, T.A. Arctic Sea Ice in the First Half of the 20th Century: Temperature-Based Spatiotemporal Reconstruction. *Izv. Atmos. Ocean. Phys.* **2020**, *56*, 534–538. [[CrossRef](#)]
23. Huang, B.; Thorne, P.W.; Banzon, V.F.; Boyer, T.; Chepurin, G.; Lawrimore, J.H.; Menne, M.J.; Smith, T.M.; Vose, R.S.; Zhang, H.-M. Extended Reconstructed Sea Surface Temperature, Version 5 (ERSSTv5): Upgrades, Validations, and Intercomparisons. *J. Clim.* **2017**, *30*, 8179–8205. [[CrossRef](#)]
24. Olonscheck, D.; Mauritsen, T.; Notz, D. Arctic sea-ice variability is primarily driven by atmospheric temperature fluctuations. *Nat. Geosci.* **2019**, *12*, 430–434. [[CrossRef](#)]
25. Stroeve, J.; Notz, D. Changing state of Arctic sea ice across all seasons. *Environ. Res. Lett.* **2018**, *13*, 103001. [[CrossRef](#)]
26. Strashnaya, A.I.; Maksimenko, T.A.; Chub, O.V. Agrometeorological features of the 2010 drought in Russia compared to the droughts of previous years. *Tr. Gidrometeorol. Nauchno-Issledovatel'skogo Tsentra Ross. Fed.* **2011**, *345*, 171–188. (In Russian)
27. Grant, A.; Brönnimann, S.; Ewen, T.; Griesser, T.; Stickler, A. The early twentieth century warm period in the European Arctic. *Meteorol. Z.* **2009**, *18*, 425–432. [[CrossRef](#)]
28. Kumar, A.; Yadav, J.; Mohan, R. Spatio-temporal change and variability of Barents-Kara sea ice, in the Arctic: Ocean and atmospheric implications. *Sci. Total. Environ.* **2020**, *753*, 142046. [[CrossRef](#)] [[PubMed](#)]
29. Cai, Q.; Beletsky, D.; Wang, J.; Lei, R. Interannual and decadal variability of Arctic summer sea ice associated with atmospheric teleconnection patterns during 1850–2017. *J. Clim.* **2021**, *34*, 9931–9955. [[CrossRef](#)]
30. Bokuchava, D.D.; Semenov, V.A. The role of natural fluctuations and factors of external forcing in the Early 20th Century Warming in Northern Hemisphere. *Ice Snow* **2022**, *62*, 455–474. (In Russian)
31. Tokinaga, H.; Xie, S.-P.; Mukougawa, H. Early 20th-century Arctic warming intensified by Pacific and Atlantic multidecadal variability. *Proc. Natl. Acad. Sci. USA* **2017**, *114*, 6227–6232. [[CrossRef](#)]
32. Mokhov, I.I. Specific features of the 2010 summer heat formation in the European territory of Russia in the context of general climate changes and climate anomalies. *Izv. Atmos. Ocean. Phys.* **2011**, *47*, 653–660. [[CrossRef](#)]
33. Popova, V.V. Summertime warming in the European part of Russia and extreme heat in 2010 as manifestation of large-scale atmospheric circulation trends in the late 20th–early 21st centuries. *Russ. Meteorol. Hydrol.* **2014**, *39*, 159–167. [[CrossRef](#)]
34. Kattsov, V.M. (Ed.) *The Third Assessment Report on Climate Change and Their Consequences on the Territory of the Russian Federation*; Roshydromet: St. Petersburg, Russia, 2022; pp. 70–75. (In Russian)
35. Laine, A.; Nakamura, H.; Nishii, K.; Miyasaka, T. A diagnostic study of future evaporation changes projected in CMIP5 climate models. *Clim. Dyn.* **2014**, *42*, 2745–2761. [[CrossRef](#)]

Disclaimer/Publisher's Note: The statements, opinions and data contained in all publications are solely those of the individual author(s) and contributor(s) and not of MDPI and/or the editor(s). MDPI and/or the editor(s) disclaim responsibility for any injury to people or property resulting from any ideas, methods, instructions or products referred to in the content.